

TUTDoR

Oxidative roasting experimentation and optimum predictive model development for copper and iron recovery from a copper smelter dust.

Item Type	Article
Authors	Okanigbe, Daniel O.;Ayomoh, Michael K.;Popoola, Olawale M.;Popoola, Patricia A.;Aigbodion, Victor S.
Publisher	Elsevier B.V.
Rights	Attribution-NonCommercial-NoDerivatives 4.0 International
Download date	2026-05-09 17:07:35
Item License	http://creativecommons.org/licenses/by-nc-nd/4.0/
Link to Item	https://hdl.handle.net/20.500.14519/496



Oxidative roasting experimentation and optimum predictive model development for copper and iron recovery from a copper smelter dust



Daniel O Okanigbe, DEng (Metallurgy)^{a,**}, Michael K Ayomoh^b, Olawale M Popoola^c, Patricia A Popoola^a, Victor S Aigbodion^d

^a Tshwane University of Technology, Department of Chemical, Metallurgical and Materials Engineering, Pretoria, South Africa

^b University of Pretoria, Department of Industrial and Systems Engineering, Pretoria, South Africa

^c Tshwane University of Technology, Centre for Energy and Electric Power (CEEP), Pretoria, South Africa

^d University of Nigeria, Department of Metallurgical and Material Engineering, Enugu, Nigeria

ARTICLE INFO

Keywords:

Copper smelter dust
Optimum predictive model
Oxidative roasting
Full factorial experimental design

ABSTRACT

The success of a treatment option depends on selection of suitable process variables at which response attains optimum. Hence, this study aimed at investigating the effects of time, temperature and time-temperature on changes in mineralogy (copper sulphate (CuSO₄), copper oxide (CuO), ferrous oxide (Fe₂O₃) and ferric oxide (Fe₃O₄)) of a copper smelter dust (CSD) during oxidative roasting. This aim was achieved by 2-way analysis of variance and mathematical model development of data obtained. Results showed time as most influential factor with an optimum time of 2 hrs for the production of high yield roast products. Furthermore, it was observed that a maximum of 23.31% proportion of CuSO₄ was recovered from an input with 7.86% proportion of CuSO₄ at a temperature of 680 °C within a time frame of 2 hrs and for a furnace door opening of 25 mm. Similarly, a maximum of 18.37% of CuO was recovered from an input with 23.91% CuO at a temperature of 800 °C, for a duration of 3 hrs and 25 mm opening of the furnace door. Whereas, an optimum 0.44 ratio value of Fe₂O₃:Fe₃O₄ was recovered at a temperature 680 °C, for a duration of 2 hrs and 25 mm furnace door opening. These maximum outputs and associated experimental conditions depict optimum operating conditions of experiment. Furthermore, predicted output proportions obtained from developed constraint interpolant models were well aligned with experimental outputs. A maximum percentage error of 0.07% was recorded in the predictive output for both water and acid soluble mineral fractions.

1. Introduction

The copper smelter dust (CSD) is a potential secondary resource of copper ore. During the beneficiation of copper ore, approximately 5–10% of the total feed is lost as CSD (Okanigbe, Popoola and Adeleke, 2017) which constitutes a significant amount of the copper value in close association with impurities like bismuth, lead, arsenic and antimony (Ha et al., 2015). Hence, the treatment of this by product cannot be over-emphasized as it bothers on mineral conservation, utilization of scant copper resources and its sustainability (Guney, Onal and Atmaca, 2015). Consequent upon this, significant investigations have been carried out on the dissolution and recovery of copper value from several CSDs (Wu et al., 2015; Alguacil et al., 2015; Chen et al., 2012; Xu, Qiang and Nie, 2010; Vitková et al., 2011; Vakyabad et al., 2012; Bakhtiari and Darezeshki, 2011; Morales et al., 2010; Chen et al., 2012; Ha et al., 2015).

The acid-leach processing of CSDs and options for recovering metal values from the resultant leach solutions have been presented in some reports (Morales et al., 2010; Chen et al., 2012; Ha et al., 2015) together with sulphidization (Sahu et al., 2012) as a technique of purifying refinery and acid plant-bleed solutions. In-depth leaching studies looked at impacts of temperature, residence time, and sulphuric-acid concentration, together with the use of refinery and acid-plant-bleed solutions on the solubility of metal values in the dust. Sequential studies into leach-solution processing steps involved cooling to precipitate copper sulphate (CuSO₄), sulphur dioxide (SO₂) decrease to precipitate the arsenic trioxide, solvent extraction to take away iron, neutralization to precipitate calcium-iron arsenates, neutralization to precipitate bismuth, sulphidization to precipitate arsenic and/or copper sulphides, and cementation to recover copper (Wu et al., 2015).

However, the process option for extraction of copper from its sulphide

* Corresponding author.

E-mail address: okanigbedo@tut.ac.za (D.O. Okanigbe).

resources, often involves the use of the roast-leach process option (Gorai, Jana and Khan, 2002; Yin et al., 1992). This process option is carried out by first subjecting the copper resource to either low temperatures (partial roasting) or high temperatures (dead roasting) with the objective of producing dissolvable oxidative products (or calcines) for copper recovery (Carter et al., 1994; Magagula, 2012). The basic roasting conditions as employed in pyro-metallurgy can be either of these three following situations: 1) when the ore is completely reacted leaving a cold process, 2) when the ore is totally reacted but leaves the furnace still hot and 3) when the roasting reaction is not run to completion.

The success of a treatment option depends on the selection of suitable process variables at which the response attains its best. One of the experimental design methods used to achieve best responses is the Full Factorial Methodology (FFM), which was used to design the density separation experimentation of a CSD, for enhanced copper recovery ([13] Okanigbe et al., 2018). Additionally, there are other experimental design methods that can be used to screen relevant variables ([21]Akar sen, 2016; [1]Aslan, 2008; [22]Xiao and Vien, 2004). However, there are limited reports on optimum predictive modeling methods used in pyro-metallurgical pretreatment or treatment of secondary copper resources to determine the behaviour of copper recovery under specified conditions.

Furthermore, it is customary in pyro-metallurgy to conduct a rigorous and costly experimental evaluation of laboratory tests and/or pilot-scale equipment trials to assess the performance of the unit operation. As a result, developing a low cost, time saving tool with the ability to correctly predict the performance of these unit operation would be advantageous. A mathematical model can be used to achieve this purpose of predicting certain occurrences, while expressing it as a set of equations (Cao et al., 2018). Additionally, the optimization and development of both old and new processes can be achieved via mathematical modeling in a cost effective manner. Mathematical models have the advantage of today, because of the availability and obvious decline in the cost of hardware and software. The past few years have recorded significant achievements with the use of mathematical modeling in areas of mechanistic modeling, system modeling and the representation of distributed parameter systems. Even though in the past non-natural obstacle have been positioned between the scientists and engineers saddled with the responsibility of structure and properties of the finished product on one hand and on the other hand those focused on metals extraction and refining, i.e. the production of semi-finished products like slabs, rods, bars or billets. Apart from this obstacle being non-natural and needless, it is also positively harmful. Hence, this challenge requires a holistic approach, one capable of fully integrating the “primary”, “secondary”, and the finishing operations, in order to come to the optimal approach. Mathematical models therefore possess the capacity in bringing about such an approach (Szekely, 1988).

Hence, this present investigation will report findings from analysis of data obtained from experimental outputs, from which deductions will be reached based on changes in mineralogy and analysis of variance to determine effect of time, temperature and time-temperature on copper sulphate (SO_4^{2-}), ferrous oxide (Fe^{2+}) and ferric oxide (Fe^{3+}) content in roast products (RP) of a secondary copper resource. Afterwards, outcomes of modeling constraint formulation and simulation using Matlab software 2014 version 8.4 in order to develop an optimum predictive model will also be reported.

2. Material and methods

2.1. Material

2.1.1. Sample preparation

This CSD sample was gathered over a 7 day period during the copper smelting operation at the Palabora Copper (PTY) Ltd (PC), Limpopo, South Africa. The as-received sample was first re-weighed and subsequently homogenized by subjecting it to coning and quartering sample

Table 1

Parameters considered at three levels.

S/N	Parameters	Low (0)	Medium [1]	High [2]
X1	Roasting Temperature (C)	680	740	800
X2	Roasting Time (hr(s.))	1	2	3

Table 2

Test matrix for roasting experimentation.

Tests	Roasting Temperature (C)	Roasting Time (hr(s.))	Treatment Combination
1	0	0	00
2	0	1	01
3	0	2	02
4	1	0	10
5	1	1	11
6	1	2	12
7	2	0	20
8	2	1	21
9	2	2	22

preparation method; aliquot samples were derived from the homogenized CSD, using a rotary splitter. These aliquot samples were used for subsequent works.

2.2. Methods

2.2.1. Design of experiment (DOE)

In the present study, the FFM was used to find out the relationship among the response functions CuSO_4 , CuO and $\text{Fe}_2\text{O}_3\text{:Fe}_3\text{O}_4$ content and the two variables of the oxidative roasting (temperature and time). All the experiments were conducted using a laboratory muffle furnace in the Department of Materials science and Engineering, University of Pretoria, South Africa's pyro-metallurgical laboratory. The variables-levels considered for the test program and test matrix are given in Tables 1 and 2. To begin with, nine flat bottom type zirconium crucibles were placed in a muffle furnace set at 800 °C for 3 hrs, to determine their individual mass while empty. After which 1.2 g of the CSD were placed in the crucibles and transferred into the muffle furnace, while at room temperature (25 °C). The crucibles were placed in a straight line to each other, after which the furnace door was kept open at an angle of 45° for each test to allow supply of air into the muffle furnace during the roasting operation. The roast products of each test were collected, weighed, and analyzed for copper and iron content in form of CuSO_4 , CuO , Fe_2O_3 and Fe_3O_4 . The experimental outputs were characterized using x-ray diffractometer (XRD), ion chromatography and ultraviolet-visible spectroscopy. The data obtained were analyzed for change in mineralogy and analysis of variance to determine effect of temperature and time on roast products (RP), afterwards the results were subjected to modeling constraint formulation and simulation on Matlab software 2014 version 8.4.

2.2.2. Modeling

2.2.2.1. Modeling procedure for output prediction. This sub-section presents the basic steps utilized in the modeling process as contained in this paper:

- Step #1: Study trend of experimental samples
- Step #2: Set-up constraint models to categorize and group samples into sub-classes based on #1.
- Step #3: Compute absolute difference between input and output samples in same class as grouped in #2.
- Step #4: identify different experimental levels for selected classes.
- Step #5: Apply interpolant model to predict output
- Step #6: End

Table 3
Generalized representation of model variables.

Level	Data Acquisition Procedure	Input value for variant factor p_{ij}	Output value for variant factor p_{oj}	Expt. Levels	Absolute difference between p_{ij} and p_{oj}
1-First	Prediction	P_{i1}	P_{o1}	ξ	$ p_{i1} - p_{o1} = \Phi_1$
2-s	Experiment	P_{i2}	P_{o2}	μ	$ p_{i2} - p_{o2} = \Phi_2$
3-Third	Experiment	P_{i3}	P_{o3}	σ	$ p_{i3} - p_{o3} = \Phi_3$

Table 3 contains a generalized representation of the modeling variables. These variables were built into a model and used for the determination of the predictive outputs of the different mineral constituents as contained in the experimental concentrates. The modeling procedure herein is premised on constrained interpolation of outputs from any three sequenced experimental samples. Usually, two of these outputs are known via experimentation while the third unknown output is obtained via predictive modeling. In Table 3, the first and second columns represent the sequenced experimental trials under consideration for interpolation. The third and fourth columns respectively represent the (%) proportions of the inputs (p_{i1} , p_{i2} and p_{i3}) and outputs (p_{o1} , p_{o2} and p_{o3}) for the mineral constituents under investigation. Furthermore, column five represents the experimental levels while column six represents the absolute difference between the input and output values expressed in terms of Φ_1 , Φ_2 and Φ_3 for each of the three experimental samples under consideration.

The following under listed are modeling notations as presented in this research:

Output = f(speed, flow rate, input, feed rate, liquid solid ratio)

Let: serial number for inputs: $s_i = \{1, \dots, n - 1, n\}$ and serial number for outputs: $s_o = \{1, \dots, n - 1, n\}$ for $\forall n \in R$ where:

$exp_{(i)ij}$ = Experimental inputs

$exp_{(o)ij}$ = Experimental outputs

$Pre_{(o)ij}$ = Predictive outputs

p_{ij} = % input proportion of selected samples

p_{oj} = % output proportion of selected samples

$\Delta p_j = |p_{ij} - p_{oj}|$ absolute difference between p_{ij} and p_{oj} where: $j = \{1, \dots, k - 1, k\}$ represents experimental levels.

The “absolute difference” models expressed in terms of the experimental levels are as presented in Ref. [1–3] while [4–6] with respect to Table 3 represent the final computational models for predicting the unknown outputs.

$$\Phi_1 = \left[\frac{\Phi_3(\mu - \xi) - \Phi_2(\mu - \xi) - \Phi_2(\sigma - \mu)}{(\mu - \sigma)} \right] \tag{1}$$

$$\Phi_2 = \left[\frac{\Phi_3(\mu - \xi) + \Phi_1(\sigma - \mu)}{(\sigma - \mu) + (\mu - \xi)} \right] \tag{2}$$

$$\Phi_3 = \left[\frac{\Phi_1(\mu - \sigma) + \Phi_2(\sigma - \mu) + \Phi_2(\mu - \xi)}{(\mu - \xi)} \right] \tag{3}$$

$$|p_{i1} - p_{o1}| = \Phi_1 \tag{4}$$

$$|p_{i2} - p_{o2}| = \Phi_2 \tag{5}$$

$$|p_{i3} - p_{o3}| = \Phi_3 \tag{6}$$

Hence, $\Delta p_j = \Phi_j$

3. Results and discussion

3.1. Oxidative roasting experimentation

3.1.1. Effect of roasting on $CuSO_4$ content

The XRD results in Fig. 1 show that copper sulphate ($CuSO_4$) content is highest at 2 hrs of oxidative roasting, but declines as the time extends to 3 hrs, however, being most insignificant at temperature of 800 °C; where the total amount of $CuSO_4$ minerals (Antlerite and Dolerophane) produced after 2 hrs is 7.95 wt% but dropped significantly to 0.52 wt% after 3 hrs.

Two-way analysis of variance was carried out on the data obtained from chemically analyzing the RP for ionic species. The results obtained

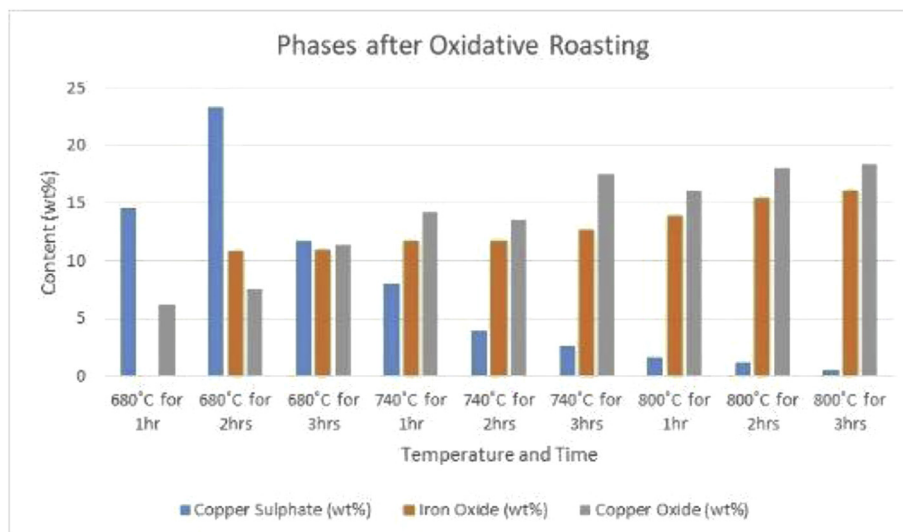


Fig. 1. Mineralogy of roasted CSD.

Table 4
Two-way analysis of variance for SO_4^{2-} concentration.

Source	Partial SS	df	MS	F	Prob > F
Model	3327.74013	8	415.967516	2.45	0.0544
Time	1397.1698	2	698.584901	4.12	0.0337
temperature	407.324311	2	203.662156	1.20	0.3240
Time/temperature	1523.24601	4	380.811503	2.24	0.1046
Residual	3053.32828	18	169.629349		
Total	6381.0684	26	245.425708		

Table 5
Tukey- Kramer pairwise comparisons for time studentized range critical value (0.05, 3, 18) = 3.6093535.

Group vs Group	Mean	mean	difference	TK-test
0 vs 1	33.6344 ^[0]	37.8578 ^[1]	4.2233	0.9728
0 vs 2	33.6344 ^[0]	20.9311 ^[2]	12.7033	2.9261
1 vs 2	37.8578 ^[1]	20.9311 ^[2]	16.9267	3.8989*

Table 6
Two-way analysis of variance for Fe^{2+} .

Source	Partial SS	df	MS	F	Prob > F
Model	1.219785260	8	0.152473157	6.71	0.0004
Time	1.029099020	2	0.514549509	22.65	0.0000
temperature	0.053738740	2	0.026869370	1.18	0.3292
Time/temperature	0.136947501	4	0.034236875	1.51	0.2421
Residual	0.408922671	18	0.022717926		
Total	1.628707930	26	0.062642613		

Table 7
Tukey- Kramer pairwise comparisons for time studentized range critical value (0.05, 3, 18) = 3.6093535.

Group vs Group	Mean	Mean	difference	TK-test
0 vs 1	0.9250 ^[0]	0.6583 ^[1]	0.2667	5.3077*
0 vs 2	0.9250 ^[0]	0.4479 ^[2]	0.4771	9.4963*
1 vs 2	0.6583 ^[1]	0.4479 ^[2]	0.4771	4.1887*

show the effects of temperature and time on change in mineralogy of CSD. As observed in Table 4, the combined effect of temperature and time on the concentration of SO_4^{2-} in the RP was not significant at $p = 0.1046$; furthermore, the effect of temperature alone was not significant at $p = 0.3240$. However, the effect of time was observed to be significant at $p = 0.0337$, which was lower than the model's p-value of 0.0544. The RP with highest concentration of SO_4^{2-} were observed between 2 hrs and 3 hrs at a temperature of 680 °C (Table 5).

3.1.2. Effect of roasting on ferrous ion (Fe^{2+}) and ferric ion (Fe^{3+}) contents

3.1.2.1. Concentration of Fe^{2+} . The XRD results (Fig. 1), shows that the amount of Fe_2O_3 was at its highest after 1hr and often at its low after 2 hrs while increasing after 3 hrs of oxidative roasting.

The combined effect of temperature and time on the concentration of Fe^{2+} in the oxidative products of the CSD from PC is not significant at 0.2421; whilst the marginal effect of temperature is not significant at $p = 0.3292$ (Table 6). However, the concentrations of Fe^{2+} at different time periods differ from each other, such that the Fe^{2+} with the highest difference was observed between 1hr and 2 hrs (Table 7).

3.1.2.2. Concentration of Fe^{3+} . The XRD results in Fig. 1 shows that the Fe_3O_4 content (wt%) between 1 hr and 2 hrs is double more than the difference between 1 hr and 3 hrs. Even though these differences were observed at 680 °C and 800 °C alone.

The combined effect of temperature and time on the concentration of

Table 8
Two-way analysis of Variance for ferric Fe^{3+} .

Source	Partial SS	df	MS	F	Prob > F
Model	3.349274980	8	0.418659373	2.88	0.0295
Time	2.503136580	2	1.251568290	8.62	0.0024
temperature	0.065713400	2	0.032856700	0.23	0.7997
Time/temperature	0.780425003	4	0.195106251	1.34	0.2922
Residual	2.613053290	18	0.145169627		
Total	5.962328270	26	0.229320318		

Table 9
Tukey- Kramer pairwise comparisons for time studentized range critical value (0.05, 3, 18) = 3.6093535.

Group vs Group	Group mean	Group mean	difference	TK-test
0 vs 1	2.2790	2.9917	0.7127	5.6114*
0 vs 2	2.2790	2.8258	0.5468	4.3052*
1 vs 2	2.9917	2.8258	0.1659	1.3062

Fe^{3+} in RP is not significant at $p = 0.2922$ (Table 8). The marginal effect of temperature is also not significant at $p = 0.7997$. The concentration of Fe^{3+} at different time periods differ significantly from each other, such that the concentration of Fe^{3+} in the RP, produced at 1 hr and 2 hrs and that produced at 1 hr and 3 hrs differ significantly from each other, with the highest difference observed between 1 hr and 2 hrs (Table 9).

Roasting in metallurgy is essentially an oxidation reaction, whereas it may have several objectives; usually the principal one is removal of all or part of the sulphur from the ore. The sulphur removed forms SO_2 , with perhaps a little SO_3 , and passes off in the gases. Some of the sulphur, however, are often converted to sulphate and remain in the roasted ore. As the roasting action is usually incomplete, often purposely so, especially in the case of copper ores, some of the sulphides remain unattached and are present in the roasted ore in the same form as they existed in the raw ore (Shah and khalafalla, 1971).

Most of the resulting iron sulphide (FeS) will be oxidized, chiefly to Fe_2O_3 . Roasting requires free access of air in amounts largely in excess of those theoretically required by the roasting reactions, in order that each particle of ore may have sufficient contact with oxygen of the air. However, judging by the results from the XRD analysis (Fig. 2), it can be appreciated better as the amount of Fe^{2+} was at its highest after 1 hr and often at its low after 2 hrs while increasing after 3 hrs of oxidative roasting (Table 8). This can be further corroborated using the XRD results in Fig. 1; where double the difference in Fe^{3+} wt% between 1 hr and 2 hrs is more than the difference between 1 hr and 3 hrs. Although, these differences were observed at 680 °C and 800 °C alone.

The optimum mineralogy of the RP is therefore dependent on the equilibrium position of reacting substances, together with the rate at which equilibrium position is attained. Hence, results on mineralogy and statistical analysis of data for SO_4^{2-} , Fe^{2+} and Fe^{3+} concentration, show time as the most influential factor, compared to temperature, time-temperature. In line with the statement before, the activation energy of this CSD has been studied and reported as 38 kJ/mol (Okanigbe, Popoola and Adeleke, 2018).

3.2. Model development for copper and iron recovery from CSD

3.2.1. Different experimental conditions and constraints

This sub-section presents an expanded view of the DOE which was initially presented in the compact form in Tables 1 and 2 Apart from having the entire sample space of the DOE presented herein, additional experimental conditions with unknown percentage output proportion are also presented as seen in Table 10. These new inputs are represented in alphabetic serial order while the actual experimental conditions from the DOE are represented using numeric serial order. Different experimental trends in a sequential order were identified from Table 10 and used to

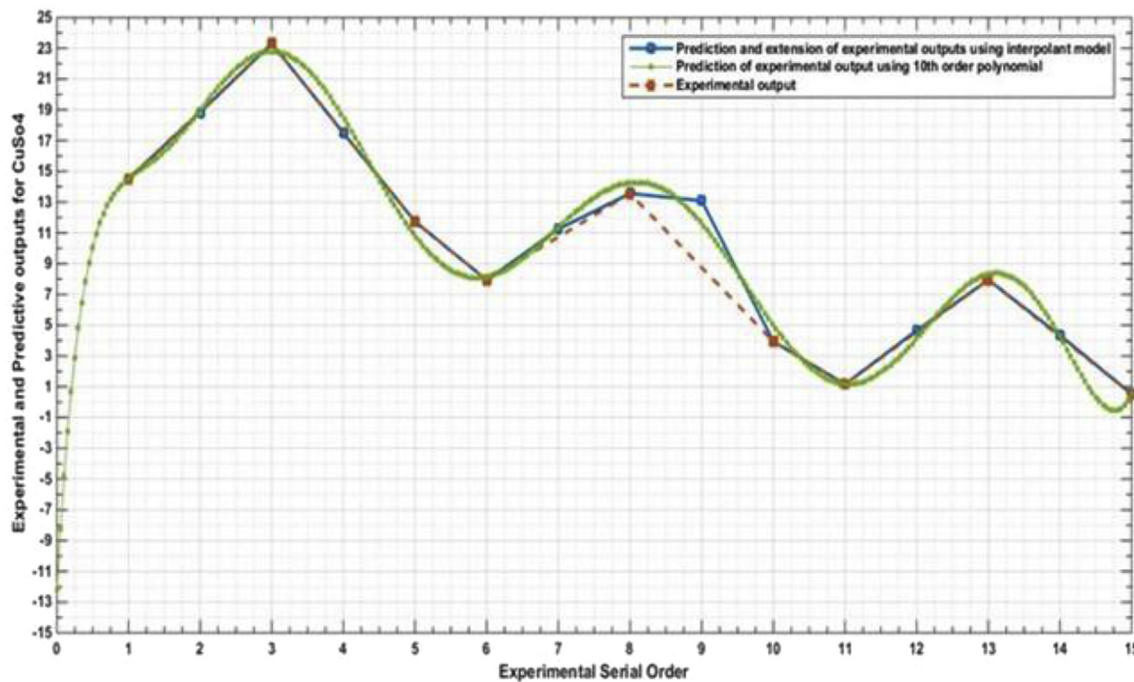


Fig. 2. Experimental and predictive output for CuSO₄.

Table 10
Inputs and Outputs data for CuSO₄, CuO and Fe₂O₃:Fe₃O₄ Content.

S/N	Input (wt%)			Process Parameters				Output (wt%)		
	CuSO ₄	CuO	Fe ₂ O ₃ :Fe ₃ O ₄	T (°C)	T (hrs)	OFR	FDO (mm)	CuSO ₄	CuO	Fe ₂ O ₃ :Fe ₃ O ₄
1	7.95	24.34	1	680	1	NC	25	14.52	6.22	0.72
A	7.82	23.97	1	680	1.5	NC	25	NE	NE	NE
2	7.86	23.85	1	680	2	NC	25	23.31	7.49	0.44
B	7.62	24.34	1	680	2.5	NC	25	NE	NE	NE
3	7.45	23.97	1	680	3	NC	25	11.72	11.37	0.43
4	8.43	24.84	1	740	1	NC	25	7.94	14.27	0.41
C	8.39	24.84	1	740	1.5	NC	25	NE	NE	NE
5	8.35	24.77	1	740	2	NC	25	13.55	16.11	0.26
D	8.31	23.93	1	740	2.5	NC	25	NE	NE	NE
6	8.29	23.93	1	740	3	NC	25	3.94	17.55	0.20
7	7.90	24.61	1	800	1	NC	25	1.16	18.06	0.18
E	8.11	24.89	1	800	1.5	NC	25	NE	NE	NE
8	8.11	24.89	1	800	2	NC	25	7.95	16.07	0.15
F	8.31	23.91	1	800	2.5	NC	25	NE	NE	NE
9	8.31	23.91	1	800	3	NC	25	0.52	18.37	0.12

Key: FeO = Fe₂O₃, Fe₃O₄; PC= Parameters considered; T = temperature; t = time; OFR= Oxygen flow mm rate; FDO= Furnace Door Opening; EO = Experimental output; PO=Predictive Output; %E = Percentage Error; NC = Not Controlled; NE = No Experiment was performed in the affected rows hence they were included for better predictive modeling intervals.

develop a set of constraint models as presented in the following sub-sections.

3.2.2. Modeling constraint

The constrained interpolant models presented in this sub-section ranging from equations [7–14] are focused on theoretical recovery of all experimental outputs as obtained from the design of experiment (DOE) see Tables 1 and 2 (compact sample size). An additional capability of these constrained models include ability to predict output proportions of mineral compositions not represented in the DOE. In a bid to achieve this robust predictive capability, a global optimum interval of 0.5unit deemed suitable as an upper interpolation limit was obtained via the rule of thumb considering predictions output consistency and a minimized overall number of predictive trials as major guiding factors. The interval of 0.5units was introduced to the time (t) column to effect the expanded DOE as presented in Table 11 resulting in additional non-experimented

rows with alphabetic serial numbering. Furthermore, some generic parameters common to both the CuO, CuSO₄ and Fe₂O₃:Fe₃O₄ mineral include: LSR = 0.5 and FR = 1.48 while the following notations viz: t = time; i = input; o = output and temp = temperature are also common to the constraint equations for the three mineral compositions.

3.2.2.1. Modeling constraint for [CuO] prediction. The constraint models presented in equations [7–10] were developed for prediction of percentage proportions of CuO from a mix of impurities under varying experimental conditions. Each of these equations are range specific in a sequenced order as presented in Table 10. The models herein follow the decreasing trend of % proportions of recovered CuO mineral by subtracting the computed absolute difference from the % input proportion. In Refs. [7], the constrained model includes experimental conditions ranging from serial numbers 1 to 3 of Table 11. This in addition contains two un-experimented conditions outside the DOE represented with serial

Table 11
Experimentation and Constrained Interpolant Predictive outputs for CuO and CuSO₄.

S/N	Input		PC				CuO			CuSO ₄		
	CuO	CuSO ₄	T	t	OFR	FDO	EO	PO	% E	EO	PO	% E
1	24.34/wt%	7.95/wt%	680/C	1.0/hrs	NC	25/mm	6.22	6.22	0.00	14.52	14.52	0
A	23.97/wt%	7.82/wt%	680/C	1.5/hrs.	NC	25/mm	NE	6.86		NE	18.83	
2	23.85/wt%	7.86/wt%	680/C	2.0/hrs.	NC	25/mm	7.49	7.49	0.00	23.31	23.31	0
B	24.34/wt%	7.62/wt%	680/C	2.5/hrs.	NC	25/mm	NE	9.86		NE	17.48	
3	23.97/wt%	7.45/wt%	680/C	3.0/hrs.	NC	25/mm	11.37	11.37	0.00	11.72	11.72	0
4	24.84/wt%	8.43/wt%	740/C	1.0/hrs.	NC	25/mm	14.27	14.27	0.00	7.94	7.94	0
C	24.84/wt%	8.39/wt%	740/C	1.5/hrs.	NC	25/mm	NE	15.23		NE	11.24	
5	24.77/wt%	8.35/wt%	740/C	2.0/hrs.	NC	25/mm	16.11	16.11	0.00	13.55	13.56	0.07
D	23.93/wt%	8.31/wt%	740/C	2.5/hrs.	NC	25/mm	NE	16.23		NE	13.09	
6	23.93/wt%	8.29/wt%	740/C	3.0/hrs.	NC	25/mm	17.55	17.19		3.94	3.94	0
7	24.61/wt%	7.90/wt%	800/C	1.0/hrs.	NC	25/mm	18.06	18.07	0.06	1.16	1.16	0
E	24.89/wt%	8.11/wt%	800/C	1.5/hrs.	NC	25/mm	NE	17.21		NE	4.66	
8	24.89/wt%	8.11/wt%	800/C	2.0/hrs.	NC	25/mm	16.07	16.08		7.95	7.95	0
F	23.91/wt%	8.31/wt%	800/C	2.5/hrs.	NC	25/mm	NE	16.73		NE	4.34	
9	23.91/wt%	8.31/wt%	800/C	3.0/hrs.	NC	25/mm	18.37	18.37	0.00	0.52	0.52	0

Key: PC= Parameters considered, T = temperature, t = time, OFR= Oxygen flow rate, FDO= Furnace Door Opening, EO = Experimental output, PO=Predictive Output, %E = Percentage Error, NC = Not Controlled, No Expt = No Experiment was performed in the affected rows hence they were included for better predictive modeling intervals.

numbers A and B. The outputs for these experiments follow a particular trend hence making the un-experimented conditions predictable. Similarly, equation [8] presents a constrained model covering serial numbers 4 to 6 and varying experimented times of 1 hr–3 hrs. Two un-experimented conditions are also contained in this constrained model viz: serial numbers C and D with experimental times ranging from 1 hr to 3 hrs. Following next are constrained models ranging from serial numbers 7 to 8 and 8 to 9 respectively. These models respectively address experimental times of 1 hr–2 hrs and 2 hrs–3 hrs also at a peak temperature of 800 °C.

$$\text{Predictive Model} = p_{oj} = p_{ij} - \Delta p_j$$

$$f \left(s/n, t, i, o, \text{temp} \right) = \begin{cases} s/n: & 1 \leq s \leq 3 \\ t: & 1 \leq t \leq 3 \\ i: & 24.34 \leq \text{CuO} \leq 23.97 \\ o: & 6.22 \leq \text{CuO} \leq 11.37 \\ \text{temp, constant} & = 680c \end{cases} \quad (7)$$

$$\text{Predictive Model} = p_{oj} = p_{ij} - \Delta p_j$$

$$f \left(s/n, t, i, o, \text{temp} \right) = \begin{cases} s/n: & 4 \leq s \leq 6 \\ t, & 1 \leq t \leq 3 \\ i, & 24.84 \leq \text{CuO} \leq 23.93 \\ o, & 14.27 \leq \text{CuO} \leq 17.55 \\ \text{temp, constant} & = 740c \end{cases} \quad (8)$$

$$\text{Predictive Model} = p_{oj} = p_{ij} - \Delta p_j$$

$$f \left(s/n, t, i, o, \text{temp} \right) = \begin{cases} s/n: & 7 \leq s \leq 8 \\ t, & 1 \leq t \leq 2 \\ i, & 24.61 \leq \text{CuO} \leq 24.89 \\ o, & 18.06 \leq \text{CuO} \leq 16.07 \\ \text{temp, constant} & = 800c \end{cases} \quad (9)$$

$$\text{Predictive Model} = p_{oj} = p_{ij} - \Delta p_j$$

$$f \left(s/n, t, i, o, \text{temp} \right) = \begin{cases} s/n: & 8 \leq s \leq 9 \\ t, & 2 \leq t \leq 3 \\ i, & 24.89 \leq \text{CuO} \leq 23.91 \\ o, & 16.07 \leq \text{CuO} \leq 18.37 \\ \text{temp, constant} & = 800c \end{cases} \quad (10)$$

3.2.2.2. Modeling constraint for [CuSO₄] prediction. The constraint models presented in equations [11–16] were developed for prediction of CuSO₄ percentage recovery proportion under same experimental conditions as CuO and same experimental input samples. Each of these

constraint models are range specific in a sequenced experimental order as presented in Table 10. The trend of experimental outputs in this scenario have a much higher level of inconsistency hence occasionally demanding a much small constrain modeling range coupled with the use of dual predictive models within some specific constrain brackets. In equation [11], the constrained model covered experimental conditions that ranged from serial numbers 1 to 2 of Table 11. Herein, an un-experimented condition outside the DOE was seen to be present with the nomenclature serial number A. Similarly, equation [12] presents a constrained model covering serial numbers 2 to 3 with a varied experimental time of 2 hrs–3 hrs. This also contains an un-experimented condition with an alphabetic serial number B. Furthermore, equation [13] contains experimental conditions covered within serial numbers 4 and 5 as presented in Table 10. Herein, the variation in % proportions between the input and output given as 8.43 to 8.35% (input proportions) with corresponding (output proportions) 7.94–13.55% necessitated the use of two separate predictive models to adequately depict the identified inconsistent trend. These models captured a seemingly opposite scenario where output proportions are observed to be lower than the input proportion on one hand and higher than input proportion on the other hand as the input proportion tends towards 8.35 from 8.43% proportion. These are as represented in the predictive models A and B respectively. The trend dynamics herein is such that as the % input proportion decreased across the profile, the output proportion increased. However, at the initial input phase, the corresponding outputs were lower in % proportion and grew to a much higher proportion as the input proportion decreased. The experimental conditions represented in equation [14] ranging from serial numbers 5 to 6 is also dual equation based following the level of trend inconsistency. However, unlike the case of [13], the trend variation between the input and output proportions in equation [14] is such that as the % input proportion decreases across the profile, the % output proportion synonymously decreases alongside. In addition, from equations [15,16] respectively represented in serial numbers 7 through 8 and 8 through 9, it could be observed that the output predictive models are similar with respect to modeling a consistently decreasing output proportion for every corresponding input. However, serial numbers 7 to 8, recorded a gradual output proportion increase as the experimental input proportion increased from 7.90 to 8.11% proportion while serial numbers 8 to 9 was a complete reverse. Herein, as the input proportion increased from 8.11 to 8.31% proportion, the output decreased from 7.95 to 0.52% proportion. However, in both cases, the corresponding output proportion from any one input sample was lower in % proportion.

Table 12
Experimentation and Constrained Interpolant Predictive outputs for Fe₃O₄:Fe₂O₃.

S/ N	PC	Fe ₃ O ₄ :Fe ₂ O ₃				Fe ₃ O ₄ :Fe ₂ O ₃		
		Fe ₃ O ₄ :Fe ₂ O ₃	T	t	OFR	FDO	EO	PO
1	1	680/ C	1.0/ hrs	NC	25/ mm	0.72	0.72	0.00
A	1	680/ C	1.5/ hrs	NC	25/ mm	NE	0.58	
2	1	680/ C	2.0/ hrs	NC	25/ mm	0.44	0.44	0.00
B	1	680/ C	2.5/ hrs	NC	25/ mm	NE	0.44	
3	1	680/ C	3.0/ hrs	NC	25/ mm	0.43	0.43	0.00
4	1	740/ C	1.0/ hrs	NC	25/ mm	0.41	0.39	0.00
C	1	740/ C	1.5/ hrs	NC	25/ mm	NE	0.34	
5	1	740/ C	2.0/ hrs	NC	25/ mm	0.26	0.27	0.00
D	1	740/ C	2.5/ hrs	NC	25/ mm	NE	0.23	
6	1	740/ C	3.0/ hrs	NC	25/ mm	0.20	0.20	
7	1	800/ C	1.0/ hrs	NC	25/ mm	0.18	0.19	0.06
E	1	800/ C	1.5/ hrs	NC	25/ mm	NE	0.17	
8	1	800/ C	2.0/ hrs	NC	25/ mm	0.15	0.16	
F	1	800/ C	2.5/ hrs	NC	25/ mm	NE	0.14	
9	1	800/ C	3.0/ hrs	NC	25/ mm	0.12	0.13	0.00

Key: PC= Parameters considered, T = temperature, t = time, OFR= Oxygen flow rate, FDO= Furnace Door Opening, EO = Experimental output, PO=Predictive Output, %E = Percentage Error, NC = Not Controlled, NE= No Experiment was performed in the affected rows hence they were included for better predictive modeling intervals.

$$\text{Predictive Model } = p_{oj} = p_{ij} + \Delta p_j$$

$$f \left(s/n, t, i, o, \text{temp} \right) = \begin{cases} s/n : 1 \leq s \leq 2 \\ t : 1 \leq t \leq 2 \\ i : 7.95 \leq \text{CuSO}_4 \leq 7.86 \\ o : 14.52 \leq \text{CuSO}_4 \leq 23.31 \\ \text{temp, constant} = 680c \end{cases} \quad (11)$$

$$\text{Predictive Model } = p_{oj} = p_{ij} + \Delta p_j$$

$$f \left(s/n, t, i, o, \text{temp} \right) = \begin{cases} s/n : 2 \leq s \leq 3 \\ t : 2 \leq t \leq 3 \\ i : 7.86 \leq \text{CuSO}_4 \leq 7.45 \\ o : 23.31 \leq \text{CuSO}_4 \leq 11.72 \\ \text{temp, constant} = 680c \end{cases} \quad (12)$$

$$\text{Predictive Model (A)} = p_{oj} = p_{ij} - \Delta p_j$$

$$\text{Predictive Model (B)} = p_{oj} = p_{ij} + \Delta p_j$$

$$f \left(s/n, t, i, o, \text{temp} \right) = \begin{cases} s/n : 4 \leq s \leq 5 \\ t : 1 \leq t \leq 2 \\ i : 8.43(A) \leq \text{CuSO}_4 \leq 8.35(B) \\ o : 7.94(A) \leq \text{CuSO}_4 \leq 13.55(B) \\ \text{temp, constant} = 740c \end{cases} \quad (13)$$

$$\text{Predictive Model (A)} = p_{oj} = p_{ij} + \Delta p_j$$

$$\text{Predictive Model (B)} = p_{oj} = p_{ij} - \Delta p_j$$

$$f \left(s/n, t, i, o, \text{temp} \right) = \begin{cases} s/n : 5 \leq s \leq 6 \\ t : 2 \leq t \leq 3 \\ i : 8.35(A) \leq \text{CuSO}_4 \leq 8.29(B) \\ o : 13.55(A) \leq \text{CuSO}_4 \leq 3.94(B) \\ \text{temp, constant} = 740c \end{cases} \quad (14)$$

$$\text{Predictive Model } : p_{oj} = p_{ij} - \Delta p_j$$

$$f \left(s/n, t, i, o, \text{temp} \right) = \begin{cases} s/n : 7 \leq s \leq 8 \\ t : 1 \leq t \leq 2 \\ i : 7.90 \leq \text{CuSO}_4 \leq 8.11 \\ o : 1.16 \leq \text{CuSO}_4 \leq 7.95 \\ \text{temp, constant} = 800c \end{cases} \quad (15)$$

$$\text{Predictive Model } : p_{oj} = p_{ij} - \Delta p_j$$

$$f \left(s/n, t, i, o, \text{temp} \right) = \begin{cases} s/n : 8 \leq s \leq 9 \\ t : 2 \leq t \leq 3 \\ i : 8.11 \leq \text{CuSO}_4 \leq 8.31 \\ o : 7.95 \leq \text{CuSO}_4 \leq 0.52 \\ \text{temp, constant} = 800c \end{cases} \quad (16)$$

3.2.2.3. Modeling constraint for [Fe₃O₄:Fe₂O₃] prediction. The constraint models presented in equations [17–19] were developed for prediction of Fe₃O₄:Fe₂O₃ percentage recovery under same experimental conditions as CuO and CuSO₄ with same experimental input samples. Each of these constraint models are range specific in a sequenced experimental order as presented in Table 10. The respective experimental percentage input and output proportions are as presented in Table 10. The constraint model presented in equation [17], covers serial numbers 1 to 3 of Table 10. Herein, two un-experimented conditions outside the DOE with alphabetic serial order A and B were added to facilitate predictive consistency using the interpolant model. The output predictive pattern as presented in the model is seen to be consistently in the downward direction.

Similarly, equation [18] presents a constrained model covering experimental conditions from serial numbers 4 to 6 in Table 10 with a varied experimental time of 1 hr–3 hrs. This also contains two un-experimented conditions with alphabetic serial order C and D and a time range of 1 hr–3 hrs. Finally is equation [19] which addresses experimental conditions covered from serial numbers 7 to 9. Herein, the temperature range is from 1 hr to 3 hrs at a temperature of 800 °C.

Whereas, the predictive modeling data presented herein for Fe₂O₃:Fe₃O₄ is from the constrained interpolant model as shown in Table 12 below. The associated experimental conditions covered herein include such conditions as presented under Table 12. Hence, if all fixed experimental conditions are held constant, the optimum experimental conditions for recovery of Fe as Fe₂O₃ and/or Fe₃O₄ from the CSD is 0.44 ratio value at a temperature of 680 °C, for a duration of 1 hr.

$$\text{Predictive Model } = p_{oj} = p_{ij} - \Delta p_j$$

$$f \left(s/n, t, i, o, \text{temp} \right) = \begin{cases} s/n : 1 \leq s \leq 3 \\ t : 1 \leq t \leq 3 \\ i : 1 \\ o : 0.72 \leq \text{Fe}_3\text{O}_4 : \text{Fe}_2\text{O}_3 \leq 0.43 \\ \text{temp, constant} = 680c \end{cases} \quad (17)$$

$$\text{Predictive Model } = p_{oj} = p_{ij} - \Delta p_j$$

$$f \left(s/n, t, i, o, \text{temp} \right) = \begin{cases} s/n : 4 \leq s \leq 6 \\ t : 1 \leq t \leq 3 \\ i : 1 \\ o : 0.41 \leq \text{Fe}_3\text{O}_4 : \text{Fe}_2\text{O}_3 \leq 0.20 \\ \text{temp, constant} = 740c \end{cases} \quad (18)$$

$$\text{Predictive Model } = p_{oj} = p_{ij} - \Delta p_j$$

$$f \left(s/n, t, i, o, \text{temp} \right) = \begin{cases} s/n : 7 \leq s \leq 9 \\ t : 1 \leq t \leq 3 \\ i : 1 \\ o : 0.18 \leq \text{Fe}_3\text{O}_4 : \text{Fe}_2\text{O}_3 \leq 0.12 \\ \text{temp, constant} = 800c \end{cases} \quad (19)$$

A 10th order polynomial model as presented in equations [18,19] was adjudged the best fit for trend analysis of the experiments conducted in

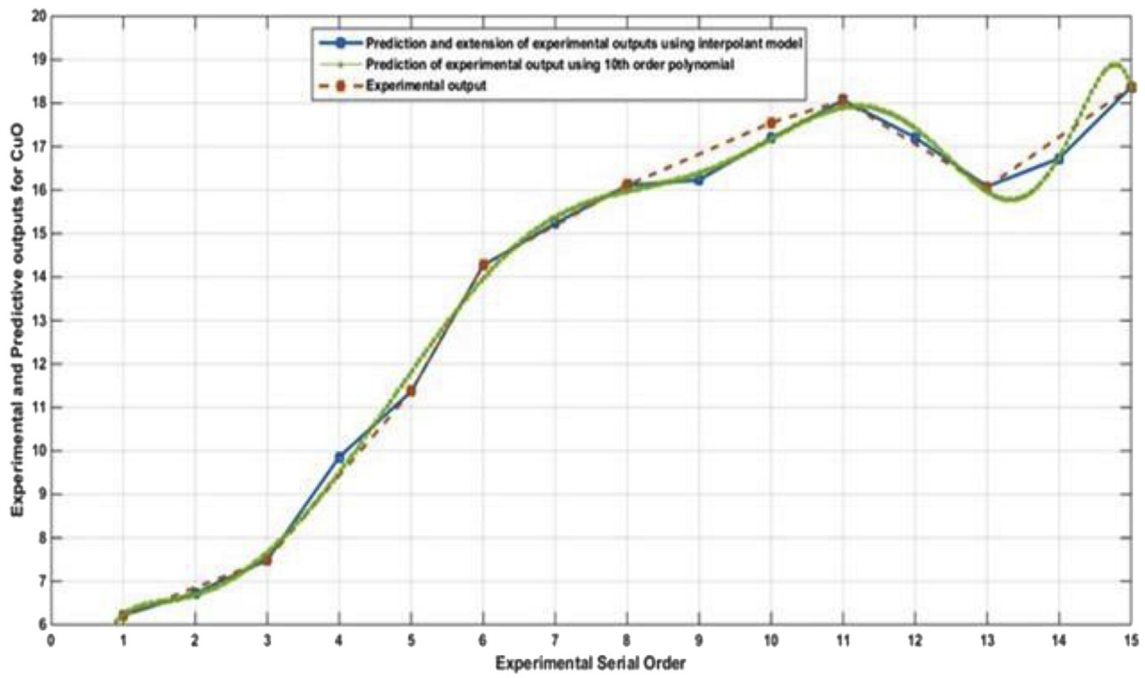


Fig. 3. Experimental and predictive output for CuO.

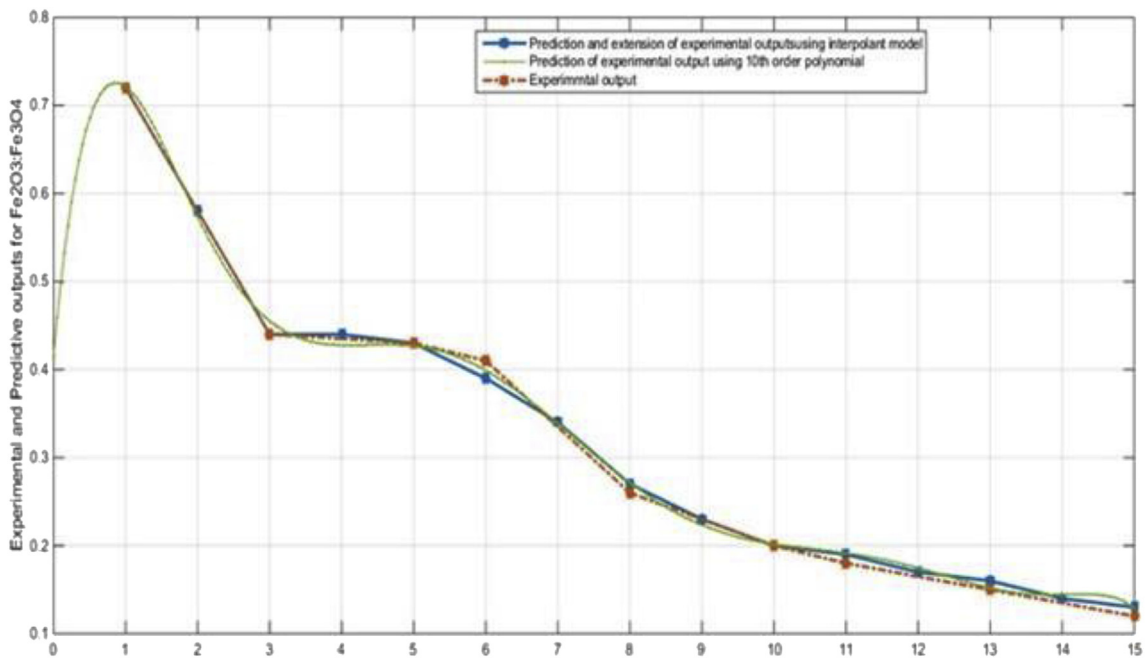


Figure 3: Experimental and Predictive Output for Fe₂O₃:Fe₃O₄

Fig. 4. Experimental and predictive output for Fe₂O₃:Fe₃O₄.

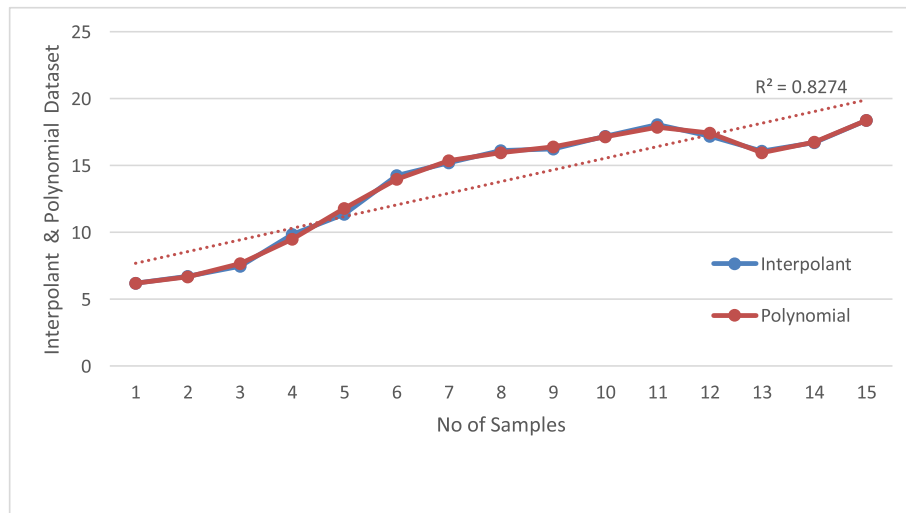


Fig. 5. Correlation coefficient for constrained interpolant and polynomial model (CuO).

this paper for CuO, CuSO₄ and Fe₂O₃:Fe₃O₄. While [17] represents a generalized form of the polynomial function [18,19], and (21) are specific functions with respect to the compounds CuO, CuSO₄ and Fe₂O₃:Fe₃O₄ respectively. Equation [20] represents the generalized form of the polynomial function for Fe₂O₃:Fe₃O₄.

$$y = P_1x^{10} + P_2x^9 + P_3x^8 + P_4x^7 + P_5x^6 + P_6x^5 + P_7x^4 + P_8x^3 + P_9x^2 + P_{10}x + P_{11} \pm e \tag{17}$$

CuSO₄

$$y = -1.2e - 06x^{10} + 9.8e - 05x^9 - 0.0035x^8 + 0.069x^7 - 0.82x^6 + 6x^5 - 27x^4 + 72x^3 - 1.1e + 02x^2 + 82x - 12 \pm e \tag{18}$$

CuO

$$y = 2.8e - 07x^{10} + 2e - 05x^9 - 0.00063x^8 + 0.011x^7 - 0.11x^6 + 0.77x^5 - 3.5x^4 + 10x^3 - 18x^2 + 17x - 0.55 \pm e \tag{19}$$

$$y = -P_1x^8 + P_2x^7 - P_3x^6 + P_4x^5 - P_5x^4 + P_6x^3 - P_7x^2 + P_8x + P_{11} \pm e \tag{20}$$

Fe₃O₄:Fe₂O₃

$$y = -3.1e - 07x^8 + 2.1e - 05x^7 - 0.00058x^6 + 0.0086x^5 - 0.073x^4 + 0.35x^3 - 0.87x^2 + 0.89x + 0.42 \pm e \tag{21}$$

where, e = error_factor

In this research, the major governing variables used in categorizing the constraint models into sub-groups are the experimental time (t) and experimental outputs. Also, a predictive interval of 0.5 was utilized as an

optimal value for the varying factor as shown in Table 10 under the time (hrs) column. The initial experimental intervals of “1 hr” as presented in the DOE for time isn’t effective to accurately predict outputs for this experiment on the long run. This has led to the introduction of new intervals of 0.5units as presented under the time column in Table 10. Validation has shown that 0.5 and lesser values would adequately satisfy the condition of predictive optimality in this research. At very low predictive intervals, wrong experimental outputs can be tracked when the discrepancy between the predicted and experimental is obviously wide apart. The effectiveness of the predicted outputs as presented for CuO, CuSO₄ and Fe₂O₃:Fe₃O₄ can be seen to be of extremely low error intervals

as shown in the percentage error column. Predicted outputs without corresponding experimental trials as seen in serial numbers (rows): A, B, C, D, E and F are considered to be with a high level of reliability and can

be used for effective planning.

The predictive outputs presented in Table 10 were obtained using an interpolant interval of 0.5 units as shown under the time (t) column of Tables 10 and 11. The simulations carried out on the developed models were conducted using MATLAB 7.1 software. The maximum error obtained between the predicted and experimental outputs was 0.07% proportion. This is contained in serial number 5 of Table 10 and under the CuSO₄ predictive column. The experimental output herein is 13.55 wt% while the predicted is 13.56 wt%. In addition, Figs. 2–4 present a graphical representation of the experimental outputs, predicted output based on the developed interpolation model and predicted output based on the fitted model from polynomial functions. These were plotted against the experimental serial order which also depicts the ordering of the temperature (C) and time (hrs) as presented in Table 11. The

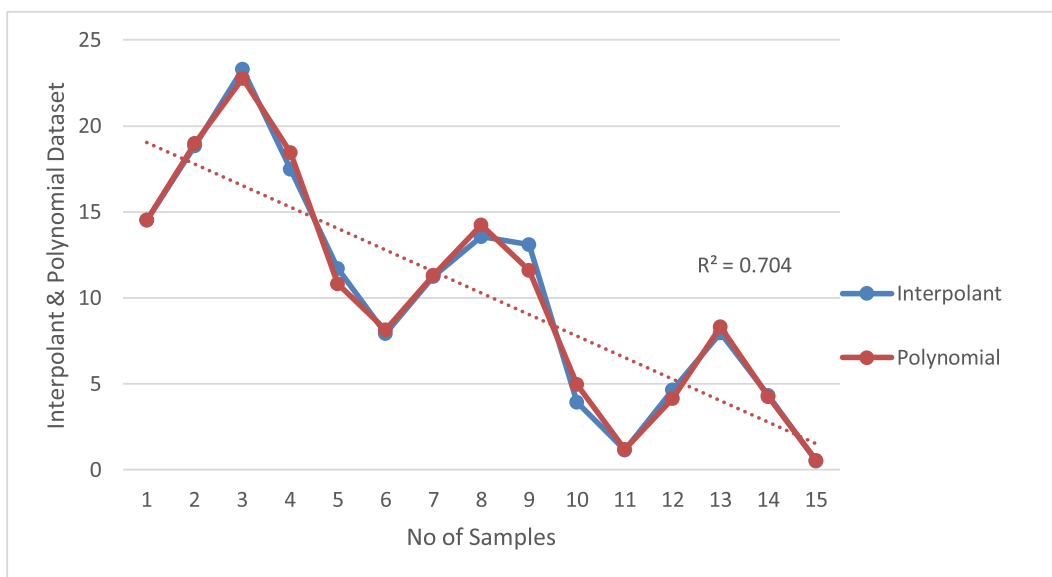


Fig. 6. Correlation coefficient for constrained interpolant and polynomial model (CuSO₄).

graphical trend for CuSO₄ as contained in Fig. 2 presented an overall least output of 0.52% proportion which occurred at temperature conditions of 800 °C and experimental duration of 3 hrs.

Furthermore, performance output proportion was highest for CuSO₄ as the temperature conditions decreased at an average time condition of 2 hrs in a time range of 1hr–3 hrs. The global peak conditions for Fig. 2 was recorded as 23.31% proportions at experimental conditions of 680 °C temperature for duration of 2 h as also shown in Table 10. Other peaked output points referred to as local peaked points includes 13.56% proportion at a temperature of 740 °C for a period of 2 hrs and 7.95% proportion at a temperature of 800 °C also for a duration of 2 hrs. Furthermore, a global minimum output proportion within the current experimental conditions was recorded at a value of 0.51% proportions when the x (axis) was at serial number 14.8 units. Other lower output proportions characterized as local minimal outputs within the brackets of 1 hr–3 hrs for varying temperature conditions include 7.94% units at a temperature of 740 °C and 1.16% proportions at a temperature of 800 °C. Hence, if all fixed experimental conditions are held constant, the optimum experimental conditions to maximize the recovery of Cu as CuSO₄ is

achieved at a temperature of 680 °C for duration of 2 hrs.

In addition, performance output proportion was highest for CuO with a % proportion of 18.37. This copper mineral was characterized with a continuous increase in % output proportion as both the temperature and experimental time increased. The shape of this graph is consistently on the rise as seen in Fig. 3. However, a local minimal decline in output was recorded between serial numbers 11 and 13.8 on the x (axis) of Fig. 3. The associated experimental conditions covered herein include such conditions as presented under serial numbers 7 through F in Table 10. Hence, if all fixed experimental conditions are held constant, the optimum experimental conditions to maximize the recovery of Cu as CuO from a mix of mineral impurities be obtained from a temperature of 800 °C and time interval of 3 hrs.

3.2.3. Correlation analysis

A statistical correlation coefficient and root mean square error was computed for dataset generated from the constrained interpolant model and polynomial curve fitting. This was carried out for all three compounds investigated namely: CuO, CuSO₄ and Fe₃O₄:Fe₂O₃. The

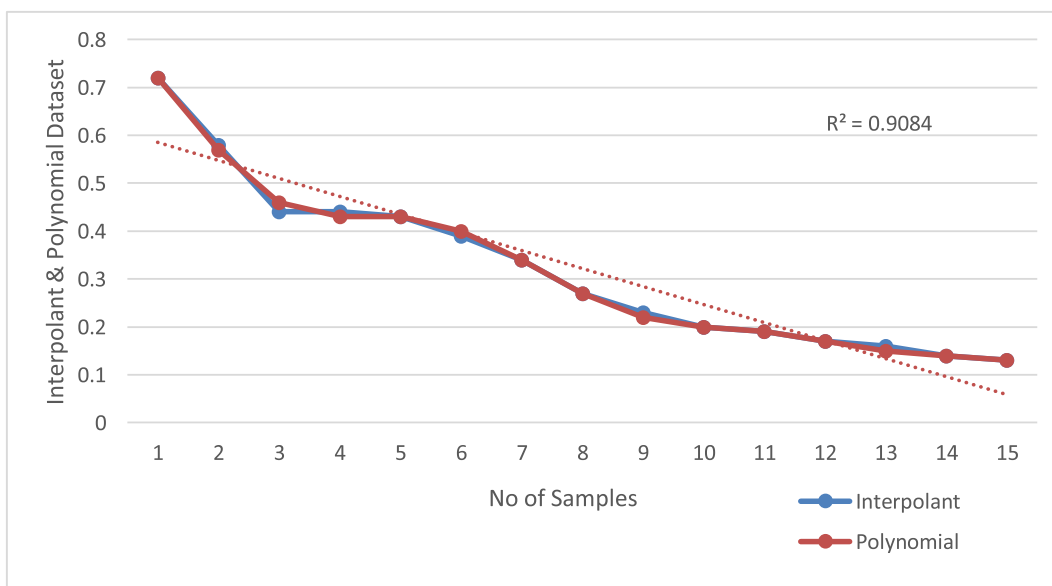


Fig. 7. Correlation coefficient for constrained interpolant and polynomial model (Fe₃O₄:Fe₂O₃).

correlation analysis graph for the trio CuO, CuSO₄ and Fe₃O₄:Fe₂O₃ is as presented in Figs. 5–7 respectively. A correlation coefficient of 0.9977 was obtained for CuO with a root mean square error of 0.200 while a correlation coefficient of 0.9901 was obtained for CuSO₄ with a root mean square error of 0.645. In the case of Fe₃O₄:Fe₂O₃ compound, the correlation coefficient obtained is 0.998 while a root mean square error of 0.0078 was obtained.

4. Conclusions

This research has presented pyro-metallurgical experimental recovery and mathematical prediction of copper and iron from CSD. Deductions leading to this point are as follows:

Although both variables considered i.e. time and temperature had influence on the mineralogy of the RP, time is however considered most influential, compared to temperature, time-temperature, and that an optimum time of 2 hrs is required for production of high-yield RP. The developed experiment specific predictive models generated outputs for un-experimented conditions beyond initial DOE. Hence, providing an authentication basis to predict the outputs of “intended experimental trials” before they are carried out or the provision of estimated output results in a situation where further experiments cannot be carried out due to fatigue, breakdown of facilities or extreme conditions of input parameters amongst others is quite relevant to this research.

The predicted output proportions obtained using the models were in good conformance with the experimental outputs. The error margins obtained were between 0.00 and 0.07%. Based on the predictive model, further outputs can be generated prior to conducting laboratory experiments. Hence, the derived models can be further used to track experimental deviations from desired plans.

Credit author statement

The conceptualization of this research was carried out by Dr Okanigbe Daniel Ogochukwu. Whereas the Data curation was carried out by Dr Okanigbe Daniel Ogochukwu after they were analyzed in the department of Geology University of Pretoria. There was no funding giving for this research other than a scholarship from Council for scientific and industrial research CSIR.

Hence, this study aimed at investigating the effects of time, temperature and time-temperature on change in mineralogy (copper sulphate (CuSO₄), copper oxide (CuO), ferrous oxide (Fe₂O₃) and ferric oxide (Fe₃O₄) of copper smelter dust (CSD) during oxidative roasting.

The methods used to achieve the aim were 2-way analysis of variance carried out in the department of mathematics and statistics Tshwane University of Technology, Pretoria, South Africa and mathematical model development using matlab 8.4 version by Dr Ayomoh Micheal, of University of Pretoria.

The manuscript was compiled and writing by Dr Okanigbe Daniel Ogochukwu, Dr Ayomoh Michael, Dr Olawale Popoola afterwards edited by Professor Popoola API.

Declaration of competing interest

There are no direct or indirect conflict of interest with respect to this research paper. Hence, the processing of this manuscript can proceed without any concern of dispute between direct and indirect parties involved.

Acknowledgement

The authors would like to thank the Council for Scientific and Industrial research (CSIR) for the financial support given to accomplish this research. Also, a special appreciation goes to Palabora Copper (PTY) Ltd, Limpopo, South Africa for providing the CSD used in this research. Finally, Tshwane University of technology, Pretoria, South Africa and the University of Pretoria, Pretoria, South Africa are duly acknowledged for providing adequate facilities and enabling environment for this research.

References

- [1] N. Aslan, Application of response surface methodology and central composite rotatable design for modeling and optimization of a multi-gravity separator for chromite concentration, *Powder Technol.* 185 (1) (2008) 80–86.
- [2] F.J. Alguacil, I. Garcia-Diaz, F. Lopez, O. Rodriguez, Recycling of copper flue dust via leaching-solvent extraction processing, *Desalination and Water Treatment* 56 (5) (2015) 1202–1207.
- [3] F. Bakhtiar, E. Darezereshki, One-step synthesis of tenorite (CuO) nano-particles from Cu₄(SO₄(OH))₆ by direct thermal-decomposition method, *Mater. Lett.* 65 (2) (2011) 171–174.
- [4] L. Cao, Y. Wang, Q. Liu, X. Feng, Physical and Mathematical Modeling of Multiphase Flows in a Converter, *Isij International*, 2018 pp.ISIJINT-2017.
- [5] M. Carter, L. Aldridge, E.R. Vance, G. Khoe, M. Zaw, Immobilisation of arsenic trioxide using cementitious materials, in: 6th AusIMM Extractive Metallurgy Conference, 1994.
- [6] Y. Chen, T. Liao, G. Li, B. Chen, X. Shi, Recovery of bismuth and arsenic from copper smelter flue dusts after copper and zinc extraction, *Miner. Eng.* 39 (2012) 23–28.
- [7] B. Gorai, R.K. Jana, Z.H. Khan, Electrorefining electrolyte from copper plant dust, *Mater. Trans.* 43 (3) (2002) 532–536.
- [8] A. Güneş, G. Önal, T. Atmaca, New aspect of chromite gravity tailings re-processing, *Miner. Eng.* 14 (11) (2001) 1527–1530.
- [9] T.K. Ha, B.H. Kwon, K.S. Park, D. Mohapatra, Selective leaching and recovery of bismuth as Bi₂O₃ from copper smelter converter dust, *Separ. Purif. Technol.* 142 (2015) 116–122.
- [10] F. Magagula, High Temperature Roasting of Sulphide Concentrate and its Effect on the Type of Precipitate Formed, *Doctoral dissertation, University of Johannesburg*, 2002.
- [11] A. Morales, M. Cruells, A. Roca, R. Bergó, Treatment of copper flash smelter flue dusts for copper and zinc extraction and arsenic stabilization, *Hydrometallurgy* 105 (1–2) (2010) 148–154.
- [12] D.O. Okanigbe, A.P.I. Popoola, A.A. Adeleke, Characterization of copper smelter dust for copper recovery, *Procedia Manuf.* 7 (2017) 121–126.
- [13] D.O. Okanigbe, A.A. Adeleke, Thermal analysis and kinetics of the oxidative roasting process of a copper smelter dust, *Int. J. Adv. Manuf. Technol.* 94 (5–8) (2018) 2393–2400.
- [14] D. Okanigbe, P. Olawale, A. Popoola, A. Abraham, A. Michael, K. Andrei, Centrifugal separation experimentation and optimum predictive model development for copper recovery from waste copper smelter dust, *Cogent Eng.* 5 (1) (2018) 1551175.
- [15] N.K. Sahu, B. Dash, S. Sahu, I.N. Bhattacharya, T. Subbaiah, Extraction of copper by leaching of electrostatic precipitator dust and two step removal of arsenic from the leach liquor, *Kor. J. Chem. Eng.* 29 (11) (2012) 1638–1642.
- [16] I.D. Shah, S.E. Khalafalla, Kinetics and mechanism of the conversion of covellite (CuS) to digenite (Cu₁₁S₈), *J. Metall. Trans.* 2 (9) (1971) 2637–2643.
- [17] J. Szekeley, The mathematical modeling revolution in extractive metallurgy, *Metal. Trans. B* 19 (4) (1988) 525–540.
- [18] A.B. Vakylabad, M. Schaffie, M. Ranjbar, Z. Manafi, E. Darezereshki, Bio-processing of copper from combined smelter dust and flotation concentrate: a comparative study on the stirred tank and airlift reactors, *J. Hazard Mater.* 241 (2012) 197–206.
- [19] M. Vítková, V. Ettler, J. Hyks, T. Astrup, B. Kříbek, Leaching of metals from copper smelter flue dust (Mufulira, Zambian Copperbelt), *Appl. Geochem.* 26 (2011) S263–S266.
- [20] Z. Yin, Copper extraction from smelter flue dust by lime-roast/ammoniacal heap leach, in: *Proceedings of the International Symposium on Residues and Effluent, Processing and Environmental Considerations*, TMS, 1992, pp. 255–266.
- [21] G. Akar Sen, Application of Full Factorial Experimental Design and Response Surface Methodology for Chromite Beneficiation by Knelson Concentrator, *Minerals* 6 (1) (2016) 5. In this issue.
- [22] Z. Xiao, Vien, A., Experimental designs for precise parameter estimation for non-linear models, *Min. Eng.* 17 (3) (2004) 431–436. In this issue.